Characterizing Degradation in Lithium-ion Batteries with Pulsing

Alan G. Li[a], Alan C. West[b], Matthias Preindl[a,*]

[a]*Department of Electrical Engineering, Columbia University in the City of New York, 500 W. 120th St., Mudd 1310, New York, NY, 10027, USA*
[b]*Department of Chemical Engineering, Columbia University in the City of New York, 500 W. 120th St., Mudd 801, New York, NY, 10027, USA*

Abstract

Degradation in lithium-ion batteries is traditionally characterized with the pseudo open-circuit voltage (pOCV) or incremental capacity (IC) but these methods have hours-long diagnostics times and cannot easily measure impedance change. It is shown here that a pulse with amplitude 1 C-rate can perform both IC and impedance characterization in just 2 minutes. Pulses and C/20 pOCV from 6 lithium-ion cells at 1328 unique combinations of state of charge, state of health, and temperature are evaluated using the convolution-defined diffusion equivalent circuit model, ridge regression, and neural networks. Ridge regression of the IC extrema and the pulse harmonics predicts SoH and nominal SoC with less than 1% and 6% error, respectively. Individual contributions of the ohmic, charge transfer, and diffusion overpotentials, as well as open-circuit voltage or hysteresis, are quantified for the charge pulse. Neural networks reconstruct IC extrema from the pulse harmonics with less than 1% error. The pulse response therefore reflects internal kinetic parameters and electrode phase transitions which are best uncovered using neural networks. Our results extend the uses of pulsing and suggest novel methods for degradation diagnostics in battery management systems.

Keywords: Lithium batteries, Overpotentials, Degradation, Incremental capacity, Pulse characterization

1. Introduction

Non-invasive and minimally-disruptive lithium-ion battery (LIB) characterization is key to effective battery management. Though advances in LIB diagnostics have enabled real-time state-of-charge (SoC) estimation, capacity fade estimation with state-of-health (SoH) requires longer time scales. Furthermore, LIB degradation results from numerous coupled internal and external mechanisms that cannot be easily observed

---

*Corresponding author.
Email address:* matthias.preindl@columbia.edu (Matthias Preindl)

Nomenclature

Abbreviations

CDD	Convolution-defined diffusion
ECM	Equivalent circuit model
EIS	Electrochemical impedance spectroscopy
ICA	Incremental capacity analysis
LAM	Loss of active material
LIB	Lithium-ion battery
LLI	Loss of lithium inventory
ML	Machine learning
NE	Negative electrode
NN	Neural network
OCV	Open circuit voltage
PE	Positive electrode
PIAML	Pulse-injection-aided machine learning
pOCV	Pseduo open circuit voltage
RC	Resistor capacitor
RR	Ridge regression
SoC	State of charge
SoH	State of health

Roman symbols

a	Weighting scalar
A_D	Diffusion constant
b	Bias vector
C_n	Capacitor n
L	Total number of layers
Q	Maximum cell capacity [Ah]
q	Remaining cell capacity [Ah]
Q_0	Initial maximum cell capacity [Ah]
r	Residual vector
R^2	Coefficient of determination
R_n	Resistor n
t	Time [s]
t_p	Pulse length [s]
V	Observed voltage [V]
V_D	Diffusion overpotential [V]
V_s	Ohmic overpotential [V]
V_{ct}	Charge transfer overpotential [V]
V_{ps}	Pseudo open circuit voltage [V]
W	Feature weight matrix
w	Feature weight vector
X	Data matrix
x	Data vector
Y	Output vector
y	Output scalar

Other symbols

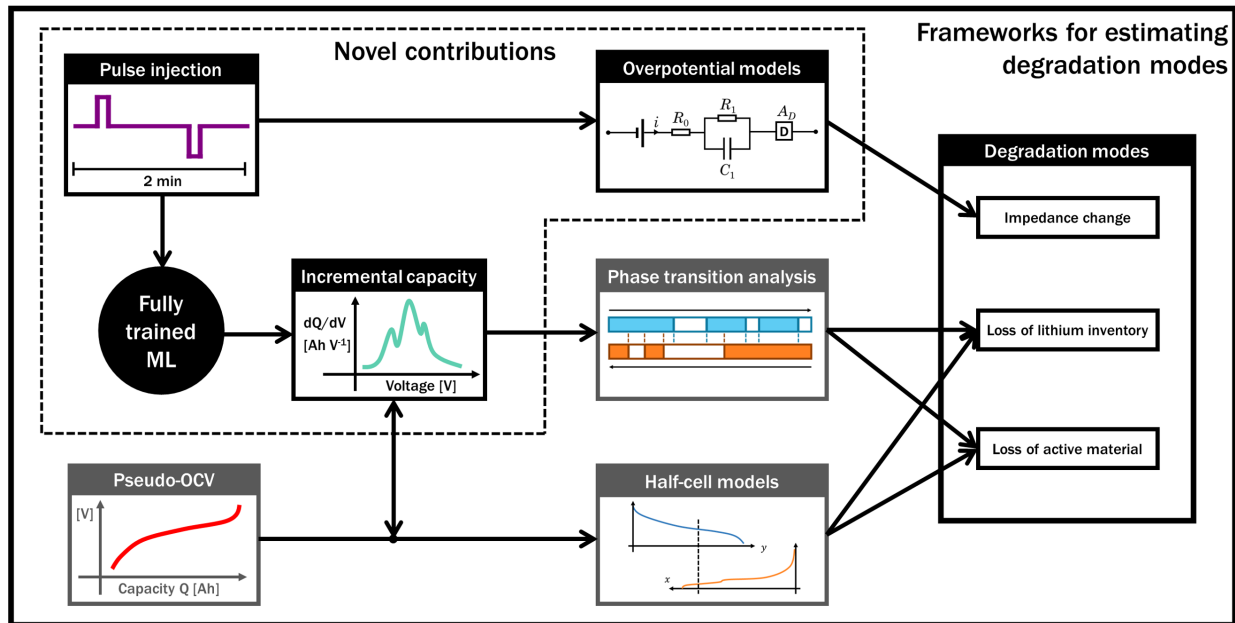|	
ℓ	Layer number
$\hat{V}$	Predicted voltage [V]
λ	Regularization parameter
$\mathcal{V}$	Voltage-time product [V·s]
σ	Activation function
θ	Parameter vector
$\tilde{v}$	Voltage harmonics [V]

Figure 1: Diagram representing frameworks for estimating degradation modes, showing novel contributions of this article

with non-invasive techniques [1, 2]. This causes considerable uncertainty in estimating the instantaneous degradation rate – an ideal quantity that remains unobservable.

Currently, LIB degradation is described using a multi-level framework containing metrics, modes, and mechanisms [3]. Each level provides more powerful diagnostics and prognostics of degradation. In theory, the modes of capacity fade such as the loss of lithium inventory (LLI) or loss of active material (LAM) can be used to determine the future SoH trajectory more accurately than just the SoH prior history. Similarly, mechanisms such as solid-electrolyte interphase formation or particle fracture are good predictors of the modes. Non-invasive techniques for multi-level characterization remain elusive, especially for modes and mechanisms.

Open-circuit voltage (OCV) or pseudo-OCV (pOCV) methods are the primary non-invasive laboratory technique for obtaining degradation modes and metrics. The pOCV curve is obtained by discharging the cell from 100% SoC at a low C-rate – defined as the current relative to the nominal cell capacity – such as C/10 or C/20 [4]. This not only yields the cell SoH but also encodes information about the positive electrode (PE) and negative electrode (NE) phase transitions. Half-cell models show that LAM and LLI may be estimated entirely from the predicted electrode degradation [5, 6]. Underpinning the results from half-cell models is incremental capacity analysis (ICA), studied extensively by Dubarry *et al.* [7, 8]. The IC curve is defined as the inverse-derivative of the pOCV with respect to remaining charge capacity. Phase transitions – plateaus
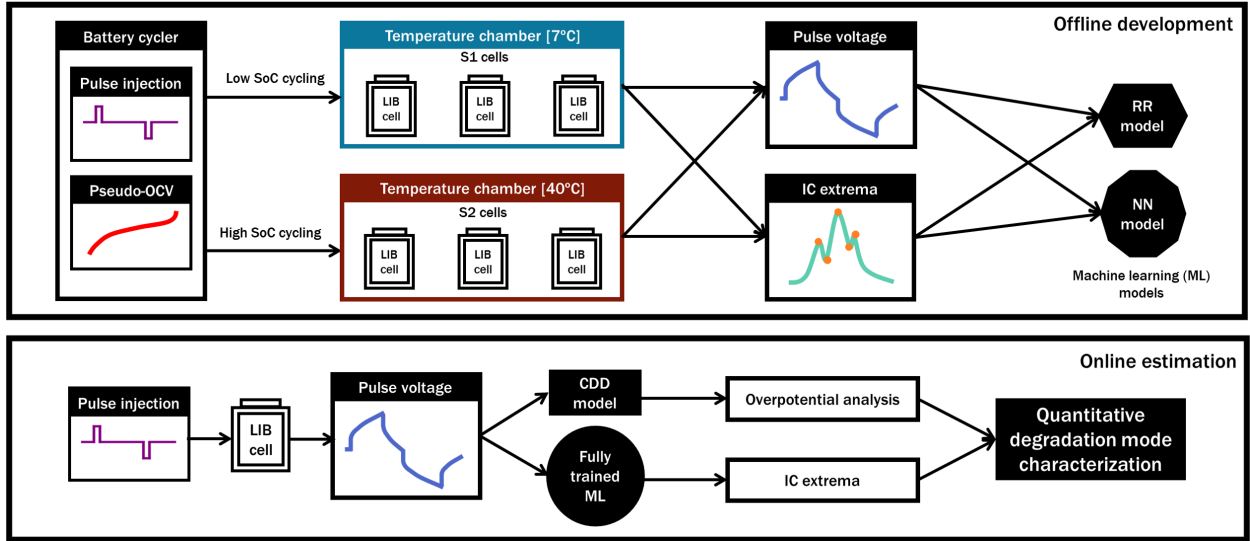
Figure 2: Diagram representing data collection and online tasks for pulse characterization with CDD-1RC model and PIAML

in the pOCV – are represented by IC extrema [9]. In many applications pOCV and ICA diagnostics are too disruptive. Though machine-learning based partial-charging methods have reduced testing time to less than an hour [10, 11, 12], and machine learning can reduce the need for pOCV acquisition [13], real-time ICA remains elusive.

Though OCV techniques can estimate modes such as LLI and LAM, impedance change is best measured with pulse perturbation [14]. It has long been used to characterize equivalent-circuit model (ECM) parameters of battery cells. Pulsing can also be used to identify overpotentials – ohmic, charge-transfer, and diffusion – when the voltage response is fitted with time-domain diffusion ECM [15]. Overpotentials are the primary cause of heat generation in LIB cells [16, 17] and reflect the kinetics of ion transport. They are thus strongly linked to degradation [18, 19, 20]. Until recently, overpotential analysis was best performed in the frequency-domain with electrochemical-impedance spectroscopy (EIS) and the Randles-Warburg ECM [21, 22]. Pulsing could provide the same information as EIS in a fraction of the time [23].

The uses of pulse perturbation extend beyond parameter identification. A neural network (NN) can accurately estimate cell states and even predict the lifetime of a LIB cell when trained on the cell's pulse voltage responses [24, 25]. This technique – named pulse-injection-aided machine learning (PIAML) – has the potential to uncover deeper levels of degradation beyond the metrics [3]. While this has been hypothesized in previous studies, the electrochemical links between pulsing and degradation are poorly defined. Hence our question — why are pulses such a powerful characterization technique?

To answer this we demonstrate our premise: that the pulse voltage response encodes signatures from ion
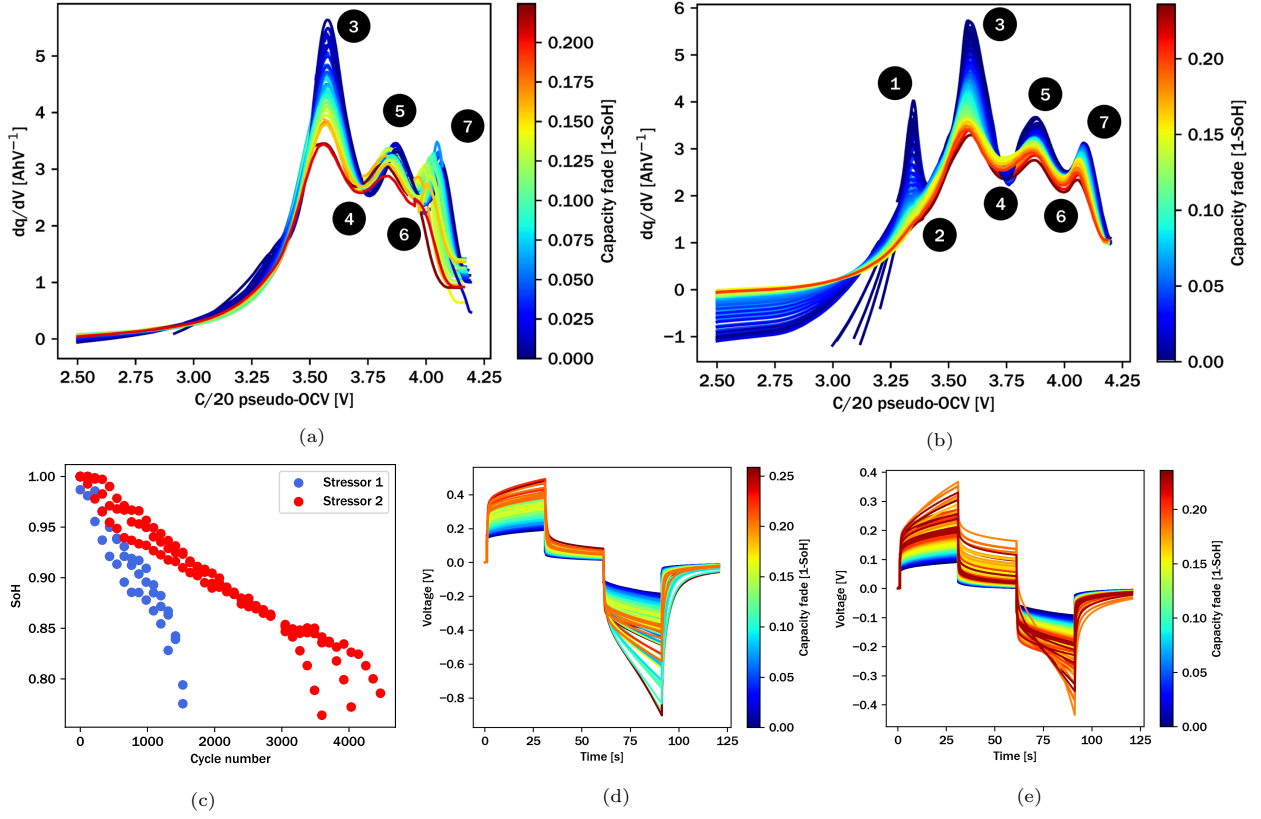
Figure 3: Data collected from six cells, showing incremental capacity curves for (a) S1 and (b) S2, (c) capacity fade for both stressors, and pulse voltage response harmonics for (d) S1 and (e) S2

transport dynamics and electrode degradation. We apply the convolution-defined diffusion (CDD) model and PIAML to experimental LIB degradation data to extract overpotential contributions, SoC, SoH, and IC features from thousands of pulses. From this we conclude that the CDD model and PIAML are sufficient to characterize degradation modes in LIB cells, as represented by our contributions to the framework in Fig. 1. This would slash degradation diagnostics time from several hours to 2 minutes.

Theoretical concepts are presented in Section 2. Results are presented and discussed in Section 3. The paper is concluded and future work described in Section 4.

2. Theory

This article explores the use of pulse injection in obtaining degradation modes. An important link between pulse injection and LLI and LAM is identified, summarized in Figs. 1 and 2. Pulse injection is traditionally only associated with impedance change. The CDD-1RC overpotential model was designed for this purpose: to accurately measure and disaggregate overpotential impedance in the cell without any prior

knowledge of the system. Ohmic, charge transfer, and diffusion overpotentials are modelled for a charge pulse with 4 parameters: R_0, R_1, C_1, and A_D [26]. While these transient dynamics are well-captured, the CDD model yields little information about the steady-state OCV behavior.

The OCV represents the equilibrium voltage attained by cell and is almost entirely determined by the lithiation of the two electrodes. As electrode lithiation fraction increases from 0 to 1, multiple phase transitions occur. Analysis of these transitions from the pOCV and IC curves yields LLI and LAM [8, 6]. By reconstructing the IC curve from pulsing, degradation diagnostics can be greatly simplified.

The experimental dataset is obtained from cells cycled with two distinct sets of stressors, named S1 and S2, represented in Fig. 2. Key diagnostics such as C/20 IC curves, capacity fade, and 1 C-rate pulse voltages are shown in Fig. 3. From the IC curves extrema points are extracted, labelled in Figs. 3(a)-(b). Each of the hundreds of pulse voltages has a unique SoH and SoC. Only pulse harmonics are used, shown in Figs. 3(d)-(e), obtained by subtracting the mean voltage from the raw pulse data. This is to eliminate effects of the OCV bias and ensure that the data only reflects overpotentials and the OCV or hysteresis variation. It may also improve data regularization.

Fundamental relationships between the data are extracted through PIAML implemented with ridge regression (RR). RR predictions are generally given by

$$y = w_{RR}^T x \tag{1}$$

where $y \in \mathbf{R}$ is the output, $w_{RR} \in \mathbf{R}^n$ is the feature vector, and $x \in \mathbf{R}^n$ is the input data vector, and n is the length of w_{RR} and x. Thus the output is a linear combination of the input data. Features are obtained using

$$w_{RR} = (\lambda I + X^T X)^{-1} X^T Y \tag{2}$$

where we choose $\lambda = 0.1$, $X \in \mathbf{R}^{m \times n}$ is the matrix of training data, $Y \in \mathbf{R}^m$ is the vector of known outputs, and m is the size of the training data, randomly selected as 80% of the total dataset. The remaining 20% of the data are used to generate predictions in Fig. 4. Results from 10 trials are shown together. For the output, SoH and SoC are considered.

Many conclusions may be drawn from Fig. 4. It can be seen from 4a that SoH is almost perfectly predicted by the IC extrema. The individual feature weights are shown in 4d. Meanwhile, SoC is predicted by pulse harmonics with 5.3% mean absolute error, shown in 4g. The most strongly weighted features as shown in 4h are located at the current step transitions, but many mid-step features are also important.
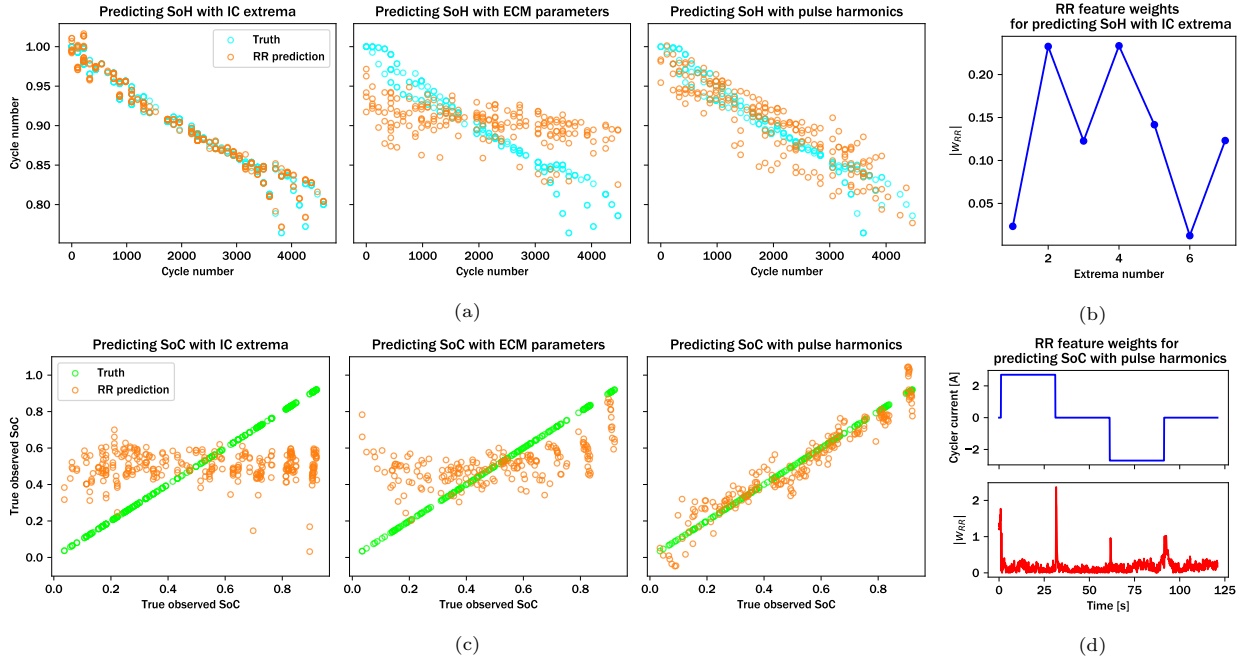
Figure 4: Plots showing ridge regression for predicting (a)-(b) SoH and (c)-(d) Nominal pulse SoC in the S2 dataset using IC extrema (column 1), CDD-1RC parameters (column 2), pulse voltage (column 3), and selected feature vectors (column 4).

These are important findings in their own right — first, that the SoH a LIB cell may be characterized by a simple linear combinations of the IC extrema; and second, that its SoC is roughly estimated without the OCV bias and with only the transient dynamics.

The ECM parameter regression results in Figs. 4 and 4 also provide useful information. They show that CDD-1RC parameters are correlated with but poor predictors of both SoH and SoC. This agrees with the known behavior of overpotentials [27]. Since they are identified using the pulse harmonics, it may be surprising that prediction accuracy from CDD parameters decreases significantly compared to direct regression of the pulse voltage. This is partially due to modelling error, but also because the pulse harmonics contain a significant characteristic not directly captured by overpotentials: OCV variation.

3. Results and Discussion

Here we demonstrate that pulses completely characterize overpotentials, OCV, and hysteresis, as well as IC curves, meaning that all degradation modes could be identified from a pulse. Results for overpotential analysis with the CDD are shown in Fig. 5. Results for IC reconstruction with PIAML are shown in Figs. 6 and 7. Generally, it can be seen that pulsing offers detailed information about battery degradation with low computational complexity.
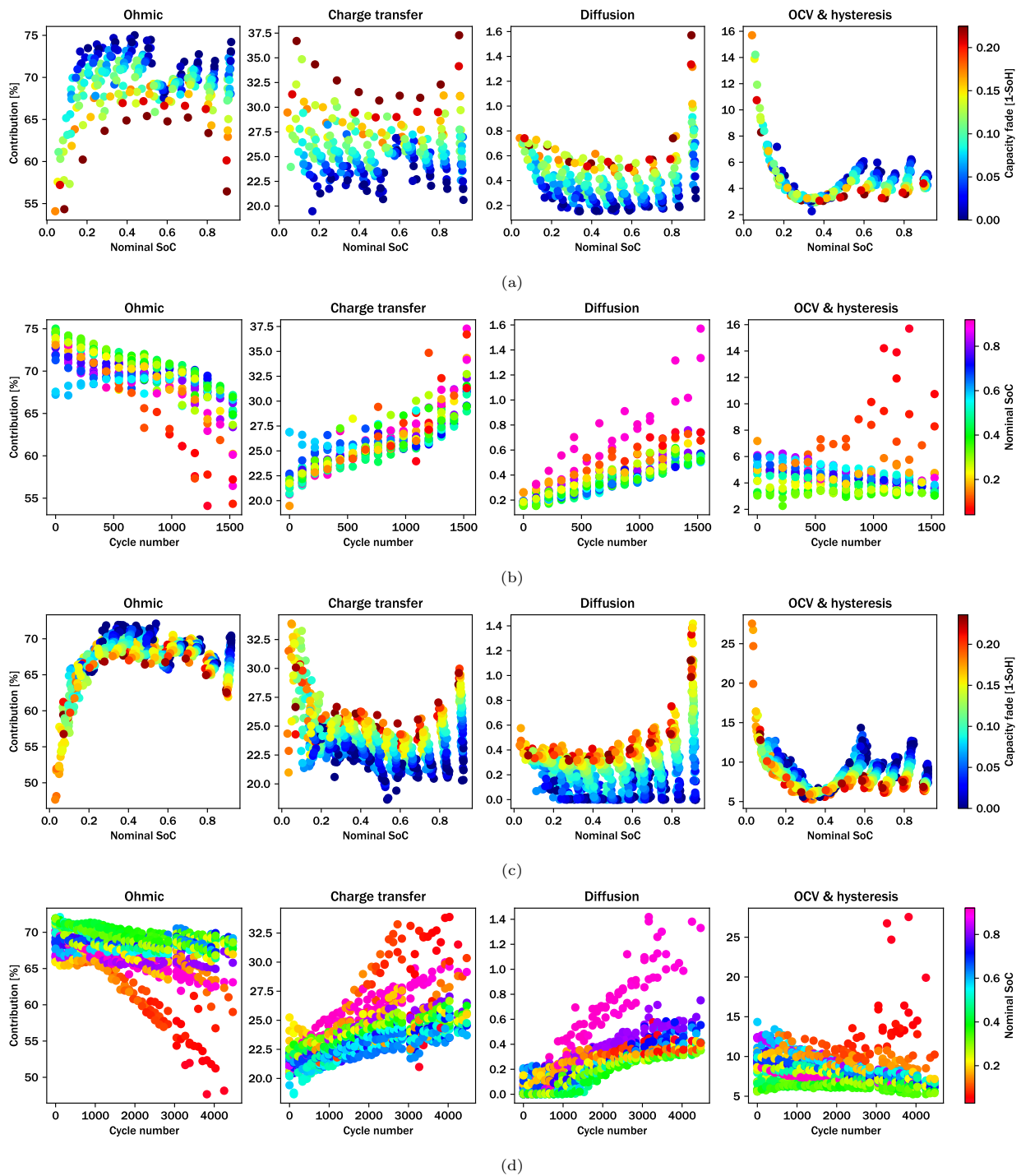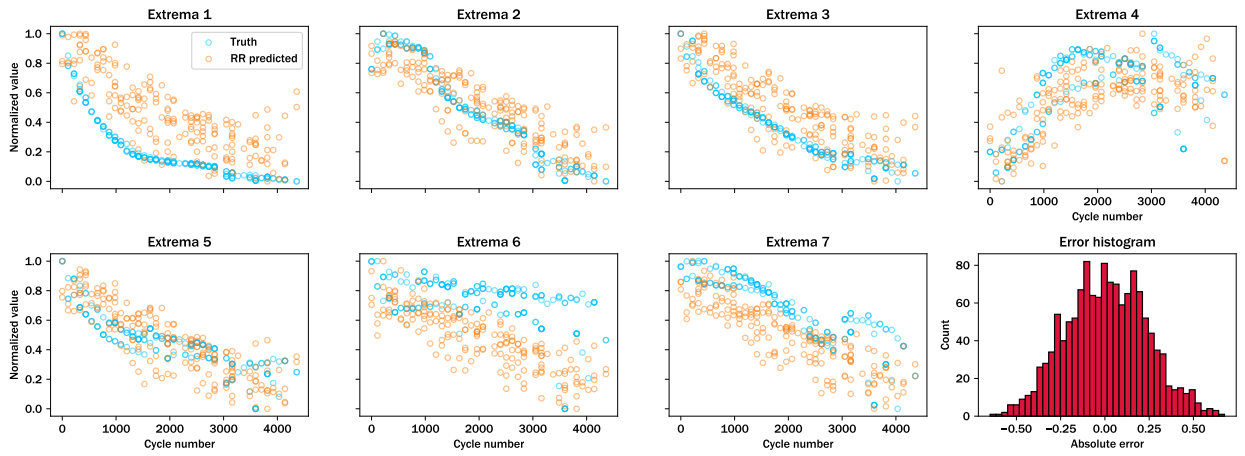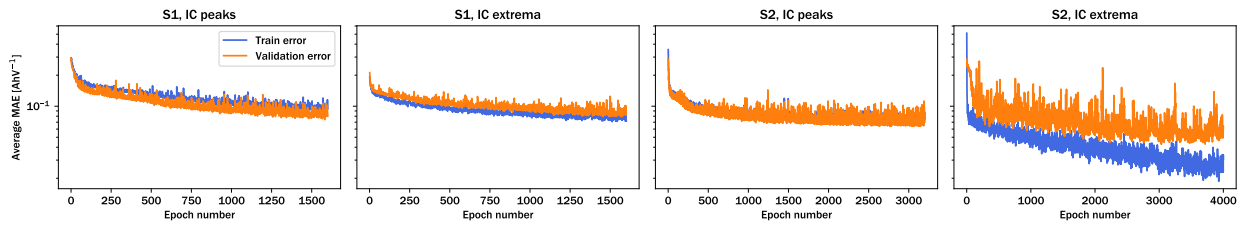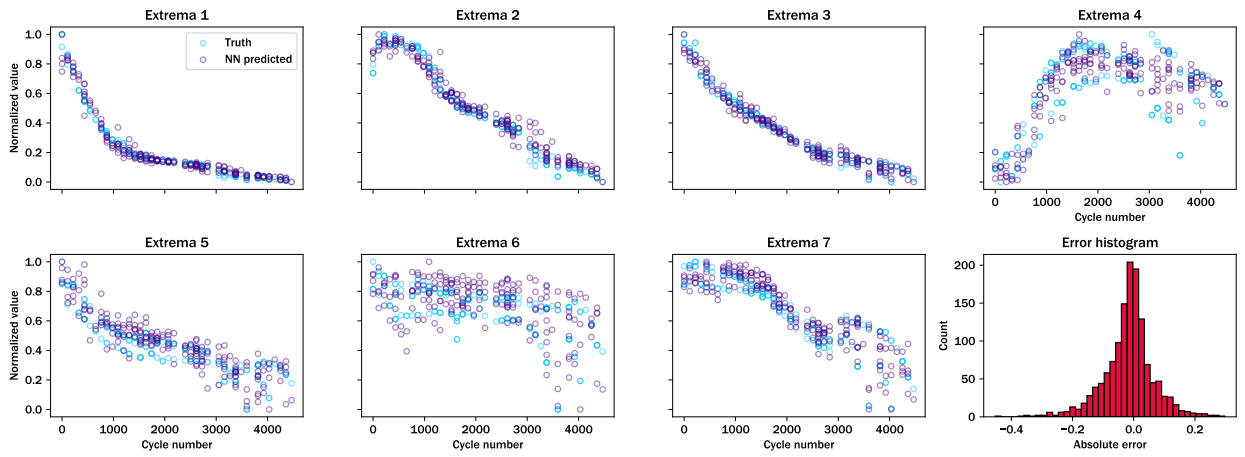
Figure 5: Overpotential contribution percentages for (a)-(b) S1 and (c)-(d) S2, showing variation against cycle number in (a) and (c) and the nominal pulse SoC in (b) and (d)

8
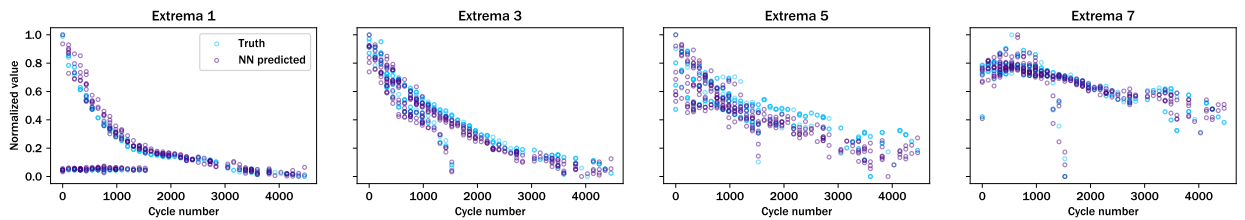
Figure 6: IC reconstruction, showing (a) RR extrema identification with the S2 dataset, (b) NN training and validation curves, (c) NN extrema identification with the S2 dataset, and (d) NN peak identification using both the S1 and S2 datasets
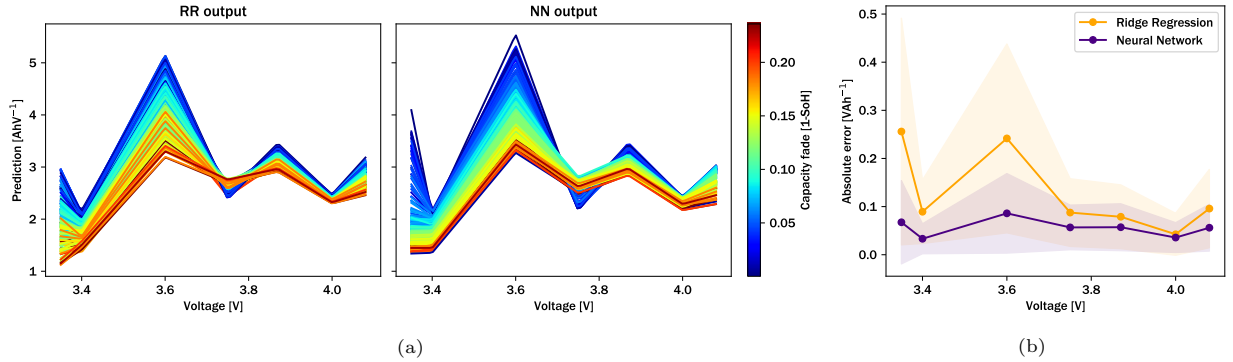
9

Figure 7: Reconstructed S2 IC curves using extrema predictions, showing outputs from (a) Ridge regression, (b) Neural network, and (c) Prediction error

Overpotential contribution percentages in the 60s charge pulse for both the S1 and S2 datasets are shown in Fig. 5, plotted against cycle number and SoC. The ohmic overpotential dominates, followed by charge transfer, OCV variation and hysteresis, and diffusion. As the cells degrade, charge transfer and diffusion become more significant. This could reflect solid-electrolyte layer formation or electrode structural change. At higher SoC, diffusion increases, corresponding to high lithiation in the NE. Charge transfer increases at low SoC, particularly evident in S2, where there is a distinct low-SoC branch beyond cycle 2000. This may reflect high lithiation in the PE impeding ion transport. OCV and hysteresis variation is calculated as the remaining voltage after subtracting the overpotentials from the observed voltage. It is particularly significant at low SoC and SoH. Peaks in the OCV contribution may reflect IC or differential voltage peaks.

ICA with RR- and NN-based PIAML is shown in Figs. 6 and 7. While RR identified a correlation between the pulse harmonics and IC extrema, it is unable to accurately reconstruct the extrema points, attaining a coefficient of determination $R^2 = 0.364$. Yet with a NN, all of the extrema points are identified with $R^2 = 0.911$. Error comparison in Fig. 7 shows that the NN is consistently more accurate and less sensitive to the peak location. The NN is also able to distinguish between stressors; in Fig. 6d the IC extrema are accurately estimated with NN-PIAML regardless of the cycling history of the cell. There must be some signature in the pulse harmonics that the NN has learnt from.

To return to our original question and explain why the IC prediction results with NN-PIAML are highly accurate, recall the RR results in Fig. 4. The inner product of the pulse voltage and a constant feature vector is a good predictor of the nominal SoC. Each SoC level therefore leaves a unique signature in the pulse. To obtain the IC curves, ML is, in a sense, tasked with predicting the cell OCV over the entire range of SoC. Whereas RR uses a feature vector to predict a single SoC, the NN uses multi-dimensional matrix transformations to obtain the entire SoC characteristic. It is hypothesized that OCV or hysteresis

Table 1: Panasonic NCR18650PF cylindrical cell specifications [28]

Characteristic	Value	Units
Positive electrode	$LiNi_{0.8}Co_{0.15}Al_{0.05}O_2$	—
Negative electrode	Carbon (graphite)	—
Rated capacity	2.7	Ah
Cut-off voltage	2.5	V
Max charge voltage	4.2	V
Cut-off current	55	mA

dynamics during the pulse, coupled with overpotentials, provide the NN sufficient information to learn the LIB cell's degradation modes. Thus the pulse harmonics have sufficient information to estimate a wide range of degradation metrics and modes — SoC, SoH, overpotentials, and IC features.

4. Conclusion

We examined the uses of pulse perturbation for diagnosing cell states, ion transport phenomena, and electrode degradation. The CDD ECM and PIAML implemented with RR and NN were applied to 1328 samples of experimental pulse data, showing that a 2 minute bipolar pulse can predict the IC features with a 0.911 coefficient of determination. To further understand the results, we disaggregate the charge pulse harmonics into 4 electrochemical dynamics and obtain a quantitative measure for each contribution.

This article extends the capabilities of PIAML diagnostics while providing greater understanding of its high performance. Several areas of research remain. Determining the optimal pulse shape, length, and amplitude could facilitate real-world implementation. PIAML may be able to characterize degradation mechanisms if each electrochemical parameter in the cell contributes a unique signature to the voltage response. In this case the NN would be an 'inverted' battery model. With deeper, more accurate, and faster degradation diagnostics, battery lifetimes and charge capacities will benefit greatly.

Methods

Data collection and processing

Six commercial Panasonic NCR18650PF cells, with specifications in Table 1, were cycled with a Neware BTS4000 series 5V6A cycler using two stressors. Stressor 1 (S1) cells were cycled from the lower cutoff 2.5 V to mid-voltage 3.7 V at 7°C and Stressor 2 (S2) cells were cycled from mid-voltage to the upper cutoff 4.2 V at 40°C in 25 L temperature chambers with a maximum range of [5, 60]°C. Tab temperature at the battery terminals was not considered. The constant-current cycling rate was 1 C-rate, 2.7 A. The C/20 pOCV and pulse train are obtained every 100 cycles, meaning each IC curve corresponds to multiple pulses.

Bipolar charge-rest-discharge-rest pulses are applied similarly to the galvanostatic intermittent titration technique [29], at SoC in the range [0.05, 1] with amplitude 1 C-rate, length 2 min, and sampling rate 10 Hz. There are 363 pulses for S1 and 965 for S2. As observed in Fig. 3, S1 cells pass the knee-point at 1500 cycles, while S2 cells degrade much more slowly, only passing the knee at 4000 cycles. A short break at 3000 cycles explains the discontinuity in the S2 capacity fade and overpotential plots in Fig. 5.

Cell SoH and SoC are obtained through coulomb counting. Integration of the current during the pOCV yields the time-varying maximum cell capacity $Q(t)$ so SoH is given by

$$\mathrm{SoH} = \frac{Q(t)}{Q_0} \tag{3}$$

where Q_0 is the capacity at $t = 0$. For each pulse, the nominal SoC is given by

$$\mathrm{SoC} = \frac{q(t)}{Q(t)} \tag{4}$$

where q is the remaining charge capacity. The IC is obtained by taking the inverse derivative of the pOCV V_{ps} with respect to the instantaneous

$$\mathrm{IC} = \frac{dq}{dV_{ps}} \tag{5}$$

A Savitzky-Golay filter is used for smoothing. For each IC curve the peaks and troughs (extrema) points are labelled sequentially. Since the S1 cells do not have the low-voltage peak and trough, S1 labels begin from 3. This is due to low-temperature effects — S2 cells only lose peak 1 after significant degradation. Finally, the voltage harmonics $\tilde{v}$ are obtained with

$$\tilde{v} = V - \mathrm{mean}(V) \tag{6}$$

where V is the raw observed pulse voltage vector.

Overpotential contribution analysis

The CDD-1RC model [26] is composed of 4 equivalent circuit elements that model the ohmic, charge transfer, and diffusion overpotentials, V_s, V_{ct}, and V_D, such that the terminal voltage is given by

$$\hat{V}(t) = V_{OC}(t) - V_s(t) - V_{ct}(t) - V_D(t) \tag{7}$$

where V_{OC} is the estimated OCV change during the pulse [15]. Circuit elements are fitted through the MATLAB scatter-search global optimization method [30],

$$
\begin{aligned}
\text{minimize} \quad & f(\theta) \\
\text{subject to} \quad & \theta \succ 0
\end{aligned}
\tag{8}
$$

We define

$$
\begin{aligned}
f(\theta) &= \|r\|_2^2 + a\|r'\|_2^2 \\
r(k) &= y_k - \hat{y}_k(\theta) \\
r'(k) &= r(k+1) - r(k) \\
\theta^T &= \begin{pmatrix} R_0 & R_1 & C_1 & A_D \end{pmatrix} \\
\theta_{\max}^T &= \begin{pmatrix} 1 & 1 & 3000 & 0.1 \end{pmatrix} \\
\theta_0^T &= \begin{pmatrix} 0.1 & 0.1 & 1000 & 0.01 \end{pmatrix}
\end{aligned}
\tag{9}
$$

where k indexes the vectors, θ is the parameter vector, we set the weighting $a = 1$, and r is the residual vector. Parameters are bounded by 0 with upper bounds $\theta_{\max}$ and initial guesses of θ_0.

To obtain the overpotential contributions, the voltage-time integral product $\mathcal{V}$ during the pulse is calculated for each overpotential during the charge pulse represented as

$$
\mathcal{V} = \int_0^{t_p} |V(t)| dt
\tag{10}
$$

where t_p is the pulse length, 60 s. The OCV variation and hysteresis contribution is then calculated as the voltage which has not been captured by the overpotentials,

$$
\mathcal{V}_{OC} = \int_0^{t_p} |\tilde{v}(t)| dt - \mathcal{V}_s - \mathcal{V}_{ct} - \mathcal{V}_D
\tag{11}
$$

The contribution fractions are calculated using

$$
\text{contribution fraction} = \frac{\mathcal{V}}{\mathcal{V}_{OC} + \mathcal{V}_s + \mathcal{V}_{ct} + \mathcal{V}_D}
\tag{12}
$$

Table 2: Hyperparameters and NN architecture with batch normalization

Hyperparameter	Value
Input nodes	1210
Hidden layers	2
Nodes per hidden layer	256
Output nodes	7
Total number of parameters	382186
Activation function	Swish
Network weight constraint	20
Optimizer	Adam
Learning rate	0.001
Batch size	64
Minimum training epochs	4000

Neural network design

Feedforward neural networks are popular ML tools composed of several layers of nodes, network weights, biases, and activation functions. Within the each layer the node outputs are represented as

$$x_\ell = \sigma(W_\ell x_{\ell-1} + b_\ell) \tag{13}$$

where W_i is weight matrix connecting nodes in layer $\ell - 1$ to layer ℓ, $x_{\ell-1}$ is the output vector from the previous layer, b_ℓ is the bias vector, and σ is the activation function governing node behavior. Note that $\ell = 0$ represents the input layer. Final output predictions are given by

$$\hat{y}_{NN} = W_L x_L + b_L \tag{14}$$

where L is the total number of layers.

Hyperparameters used to design the NN for IC feature estimation are shown in Table 2.It is noted that the NN architecture is 'wide' and 'shallow', with only 2 hidden layers. Data is split randomly into 64%, 16% and 20% subsets for training, validation, and testing. Training was performed using the Keras module of the Python Tensorflow package. The testing subset is used to obtain the final results and is presented to the NN as unseen inputs. For evaluation the coefficient of determination R^2 is calculated using

$$R^2 = 1 - \frac{\|Y - \hat{Y}_{NN}\|^2}{\|Y - \text{mean}(Y)\|^2} \tag{15}$$

which represents the complement of the ratio between the sum of the squared residuals and the total sum of squares.

References

[1] S. Saxena, D. Roman, V. Robu, D. Flynn, M. Pecht, Battery stress factor ranking for accelerated degradation test planning using machine learning, Energies 14 (2021).

[2] Y. Preger, H. M. Barkholtz, A. Fresquez, D. L. Campbell, B. W. Juba, J. Roman-Kustas, S. R. Ferreira, B. Chalamala, Degradation of commercial lithium-ion cells as a function of chemistry and cycling conditions, J. Electrochem. Soc. 167 (2020).

[3] A. G. Li, , A. C. West, M. Preindl, Towards unified machine learning characterization of lithium-ion battery degradation across multiple levels: A critical review, Appl. Energy 316 (2022).

[4] A. Fly, R. Chen, Rate dependency of incremental capacity analysis (dQ/dV) as a diagnostic tool for lithium-ion batteries, J. Energy Storage 29 (2020).

[5] K. S. Mayilvahanan, K. J. Takeuchi, E. S. Takeuchi, A. C. Marschilok, A. C. West, Supervised learning of synthetic big data for Li-ion battery degradation diagnosis, Batteries and Supercaps 4 (2021).

[6] C. R. Birkl, M. R. Roberts, E. McTurk, P. G. Bruce, D. A. Howey, Degradation diagnostics for lithium ion cells, J. Power Sources 341 (2017) 376–386.

[7] M. Dubarry, B. Y. Liaw, Identify capacity fading mechanism in a commercial LiFePO4 cell, J. Power Sources 194 (2009) 541–549.

[8] M. Dubarry, C. Truchot, B. Y. Liaw, K. Gering, S. Sazhin, D. Jamison, C. Michelbacker, Evaluation of commercial lithium-ion cells based on composite positive electrode for plug-in hybrid electric vehicle applications. part ii. degradation mechanism under 2 c cycle aging, J. Power Sources 196 (2012) 10336–10343.

[9] C. R. Birkl, E. McTurk, M. R. Roberts, P. G. Bruce, D. A. Howey, A parametric open circuit voltage model for lithium ion batteries, J. Electrochem. Soc. 12 (2015) A2271–A2280.

[10] J. Tian, R. Xiong, W. Shen, F. Sun, Electrode ageing estimation and open circuit voltage reconstruction for lithium ion batteries, Energy Storage Mater. 37 (2021) 283–295.

[11] S. Khaleghi, D. Karimi, S. H. Beheshti, M. S. Hosen, H. Behi, M. Berecibar, J. V. Mierlo, Online health diagnosis of lithium-ion batteries based on nonlinear autoregressive neural network, Appl. Energy 282 (2021).

[12] P. Tagade, K. S. Hariharan, S. Ramachandran, A. Khandelwal, A. Naha, S. M. Kolake, S. H. Han, Deep gaussian process regression for lithium-ion battery health prognosis and degradation mode diagnosis, J. Power Sources 445 (2020).

[13] X. Tang, Y. Wang, Q. Liu, F. Gao, Reconstruction of the incremental capacity trajectories from current-varying profiles for lithium-ion batteries, iScience 24 (2021).

[14] J. S. Edge, S. O'Kane, R. Prosser, N. D. Kirkaldy, A. N. Patel, A. Hales, A. Ghosh, W. Ai, J. Chen, J. Yang, S. Li, M. Pang, L. B. Diaz, A. Tomaszewska, M. W. Marzook, K. N. Radhakrishnan, H. Wang, Y. Patel, B. Wu, G. J. Offer, Lithium ion battery degradation: what you need to know, Phys. Chem. Chem. Physics 23 (2021).

[15] A. G. Li, K. Mayilvahanan, A. C. West, M. Preindl, Discrete-time modeling of Li-ion batteries with electrochemical overpotentials including diffusion, J. Power Sources 500 (2021).

[16] V. Talele, M. Patil, S. Panchal, R. Fraser, M. Fowler, S. Gunti, Novel metallic separator coupled composite phase change material passive thermal design for large format prismatic battery pack, J. Energy Storage 58 (2023).

[17] Y. Xie, Y. Liu, M. Fowler, M. K. Tran, S. Panchal, W. Li, Y. Zhang, Enhanced optimization algorithm for the structural design of an air-cooled battery pack considering battery lifespan and consistency, Int. J. Energy Research 46 (2022).

[18] Z. Chen, D. L. Danilov, L. H. J. Raijmakers, K. Chayambuka, M. Jiang, L. Zhou, J. Zhou, R. A. Eichel, P. H. L. Notten,

Overpotential analysis of graphite-based Li-ion batteries seen from a porous electrode modeling perspective, J. Power Sources 509 (2021).

[19] P. K. Koorata, S. Panchal, R. Fraser, M. Fowler, Combined influence of concentration-dependent properties, local deformation and boundary confinement on the migration of li-ions in low-expansion electrode particle during lithiation, J. Energy Storage 52B (2022).

[20] C. Pastor-Fernandez, K. Uddin, G. H. Chouchelamane, W. D. Widanage, J. Marco, A comparison between electrochemical impedance spectroscopy and incremental capacity-differential voltage as Li-ion diagnostic techniques to identify and quantify the effects of degradation modes within battery management systems, J. Power Sources 360 (2017) 301–318.

[21] D. Andre, M. Meiler, K. Steiner, H. Walz, T. Soczka-Guth, D. U. Sauer, Characterization of high-power lithium-ion batteries by electrochemical impedance spectroscopy. II: Modelling, J. Power Sources 196 (2011) 5349–5356.

[22] S. Gantenbein, M. Weiss, E. Ivers-Tiffé, Impedance based time-domain modeling of lithium-ion batteries: Part I, J. Power Sources 379 (2018) 317–327.

[23] A. G. Li, M. M. Wu, Y. A. Fahmy, M. Preindl, Fast time-domain impedance spectroscopy of lithium-ion batteries using pulse perturbation, IEEE Transportation Electrification Conference (ITEC) (2022).

[24] A. G. Li, W. Wang, A. C. West, M. Preindl, Health and performance diagnostics in Li-ion batteries with pulse-injection-aided machine learning, Appl. Energy 315 (2022).

[25] A. Weng, P. Mohtat, P. M. Attia, V. Sulzer, S. Lee, G. Less, A. Stefanopoulou, Predicting the impact of formation protocols on battery lifetime immediately after manufacturing, Joule 5 (2021) 1–22.

[26] A. G. Li, M. Preindl, Interpretable real-time modelling of the diffusion overpotential in lithium batteries, IEEE Trans. Transp. Elec Early Access (2023).

[27] V. J. Ovejas, A. Cuadras, State of charge dependency of the overvoltage generated in commercial Li-ion cells, J. Power Sources 418 (2019) 176–185.

[28] N. Togasaki, T. Yokoshima, Y. Oguma, T. Osaka, Prediction of overcharge-induced serious capacity fading in nickel cobalt aluminum oxide lithium-ion batteries using electrochemical impedance spectroscopy, J. Power Sources 461 (2020).

[29] J. Kim, S. Park, S. Hwang, W. Yoon, Principles and applications of galvanostatic intermittent titration technique for lithium-ion batteries, J. Electrochem. Sci. Technol. 13 (2022) 19–31.

[30] Z. Ugray, L. Lasdon, J. Plummer, F. Glover, J. Kelly, R. Marti, Scatter search and local NLP solvers: A multistart framework for global optimization, INFORMS Journal on Computing 19 (2007) 328–340.